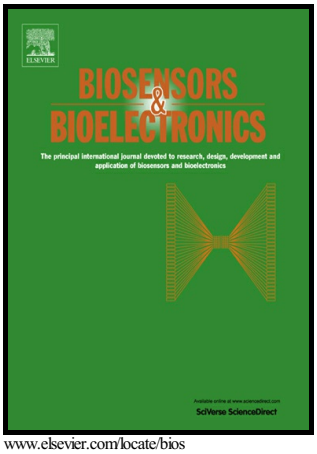

www.elsevier.com/locate/bios

Enzyme-free homogeneous electrochemical biosensor for DNA assay using toehold-triggered strand displacement reaction coupled with host-guest recognition of Fe_3O_4@SiO_2@β-CD nanocomposites

Jingjing Jiang, Xinyi Lin, Dong Ding, Guowang Diao

PII: S0956-5663(18)30291-4
DOI: https://doi.org/10.1016/j.bios.2018.04.035
Reference: BIOS10431

To appear in: *Biosensors and Bioelectronic*

Received date: 1 February 2018
Revised date: 4 April 2018
Accepted date: 16 April 2018

Cite this article as: Jingjing Jiang, Xinyi Lin, Dong Ding and Guowang Diao, Enzyme-free homogeneous electrochemical biosensor for DNA assay using toehold-triggered strand displacement reaction coupled with host-guest recognition of Fe_3O_4@SiO_2@β-CD nanocomposites, *Biosensors and Bioelectronic,* https://doi.org/10.1016/j.bios.2018.04.035

Enzyme-free homogeneous electrochemical biosensor for DNA assay using toehold-triggered strand displacement reaction coupled with host-guest recognition of Fe_3O_4@SiO_2@β-CD nanocomposites

Jingjing Jiang, Xinyi Lin, Dong Ding, Guowang Diao*

School of Chemistry and Chemical Engineering, Yangzhou University, Yangzhou 225002, PR China

*Corresponding author. Fax: +86-514-87975244. gwdiao@yzu.edu.cn

ABSTRACT

Taking advantages of the toehold-triggered strand displacement reaction (TSDR) and host-guest interaction of β-cyclodextrin (β-CD), a facile enzyme-free and homogeneous electrochemical sensing strategy was designed for the sensitive assay of target DNA using Fe_3O_4@SiO_2@β-CD nanocomposites and ferrocene-labeled hairpin DNA (H-1) as the capture and electrochemical probes, respectively. Upon addition of target molecule, the initiated TSDR process induced the conformational change of H-1, and subsequently stimulated the dynamic assembly of assist probes (A-1 and A-2) to generate H-1:A-1:A-2 duplex along with the release of target sequence. The released target could drive the next TSDR recycling and finally result in the formation of numerous DNA duplex. After the molecular recognition of Fe_3O_4@SiO_2@β-CD

nanocomposites, a large number of duplex were easily separated from the supernatant solution under an external magnetic field, which led to a decreased H-1 concentration in residual solution, concomitant with a remarkable reduction of peak current. Under the optimized conditions, wide linear range (1−5000 pM), low detection limit (0.3 pM), desirable reproducibility, good selectivity, and satisfactory practical analysis were obtained by the combination of the superior recognition capability of β-CD, TSDR-induced signal amplification, and homogeneous electroanalytical method. The proposed detection strategy could offer a universal approach for the monitoring of various biological analytes via the rational design of probe sequences.

Keywords: Homogeneous electroanalysis; Enzyme-free amplification; Toehold-triggered strand displacement reaction; Host-guest recognition; DNA bioassay

1. Introduction

The accurate readout of trace DNA sequences is crucially important for the quantitative analyses of biological markers at low level in the early stage of diseases and has a wide range of applications in molecular recognition, clinical diagnosis, and environmental monitoring (Diao et al., 2018; Zhang et al., 2014). Owing to the ever increasing requirements of highly sensitive biological assays, various signal amplification methods based on nucleases and nanomaterials have attracted considerable attention in recent years. Nucleases, such as exonuclease (Cai et al., 2014; Li et al., 2016; Shi et al., 2016), nicking endonuclease (Xu et al., 2017; Yuan et al., 2015), and polymerase (Fu et al., 2013; Li et al., 2012; Yu et al., 2014), could significantly improve the detection sensitivity by target recycling amplification techniques, which allow a target DNA molecule to hybridize with many nucleic

acid-based signal probes. However, the application prospects of nuclease-assisted amplification strategies usually suffer from some inherent disadvantages that the involved nucleases are highly sequence-specific and require strict reaction conditions to keep their activities.

To address the aforementioned problems, enzyme-free amplification approaches including catalytic hairpin assembly (CHA) (Chen et al., 2016; He et al., 2016; Hun et al., 2015), hybridization chain reaction (HCR) (Huang et al., 2011; Li et al., 2015; Liu et al., 2014), and toehold-triggered strand displacement reaction (TSDR) have shown great potentials in the sensitive detection of target analytes. TSDR is a prominent method for the construction and regulation the dynamic DNA nanostructures and nanodevices (Khodakov et al., 2013; Zhang and Seelig, 2011). In TSDR, one DNA strand in a pre-hybridized duplex is replaced by another strand to generate a more stable double-stranded complex through the stepwise branch migration induced by a short single-stranded domain termed "toehold" (typically 5−8 nucleotides) (Wang et al., 2017; Zhu et al., 2013). When the base number of toehold was changed, the kinetic rate of TSDR could be controlled over a factor of 10^6 (Zhu et al., 2014). Thus, it is highly desirable to develop TSDR-dependent nucleic acid sensing platforms for more reliable assays.

A variety of analytical techniques, such as fluorescence (He et al., 2010; Hu et al., 2014; Tan et al., 2015), colorimetry (Duan et al., 2015; Nie et al., 2014; Yu et al., 2015), electrochemistry (Xiong et al., 2017; Zhang et al., 2015), electrochemiluminescence (Chen et al., 2015; Zhang et al., 2014), photoelectrochemistry (Zang et al., 2016; Zhao et al., 2012), and surface-enhanced Raman scattering spectroscopy (He et al., 2012; Xu et al., 2015), have been extensively applied for the quantitative determination of target sequences. Among

them, the electrochemical sensing method features prominently due to its rapid response, stable signal, simple instrumentation, convenient use, low cost, and time saving (Chen et al., 2018). However, the relatively complex interface modification, multiple washing processes, and the introduction of extra exogenous reagents during the construction of heterogeneous biosensors not only result in the contamination of working electrodes, but also may decrease the amplification efficiency and fabrication reproducibility. In this context, the development of immobilization-free or homogeneous electrochemical biosensor could effectively overcome these obstacles. For example, a versatile electrochemical molecular beacon-based strategy was proposed for the direct monitoring of target analyte in a homogeneous solution phase on the basis of the exonuclease III-initiated target recycling amplification (Xuan et al., 2012). In combination of the T7 exonuclease and KF polymerase-triggered dual signal amplification method, a sensitive and immobilization-free electrochemical aptasensor was proposed for antibiotic residues determination (Wang et al., 2016). Moreover, magnetic nanoparticles as ideal carrier candidates, with large surface area and facile surface functionalization, could immobilize various active substances/capture units and quickly collect specific signal tags, which were beneficial to the design of homogeneous sensing devices (Bi et al., 2015; Li et al., 2017).

Based on this, a novel enzyme-free and homogeneous electrochemical biosensor was proposed by the integration of TSDR-assisted target recycling and flexible host-guest interaction for the sensitive assay of target DNA (Scheme 1). The as-prepared Fe_3O_4@SiO_2@β-CD nanocomposites as capture probes possessed the high recognition capability to elevate the detection sensitivity, in which Fe_3O_4 core and SiO_2 substance provided a solid support for fast magnetic separation and a stable shell layer for the effective modification of β-CD, respectively. Before target DNA

was added, the closed stem-loop structure of dual ferrocene-labeled hairpin probe (H-1) simultaneously hindered the TSDR process and the host-guest recognition of β-CD due to the principle of dimension matching (Fig. S1 in the Supporting Information). After the magnetic separation treatment, the supernatant solution containing numerous ferrocene-labeled H-1 generated a strong current response. Upon addition of target molecule, the hybridization between H-1 and the target sequence triggered the assist probes (A-1 and A-2) to further produce H-1:A-1:A-2 duplex via the TSDR process, and consequently resulted in the release of target DNA, which was allowed to start the next TSDR recycling. Finally, the cyclic utilization of a target strand could continuously open many H-1 substrates. Through the host-guest recognition between DNA duplex and Fe_3O_4@SiO_2@β-CD, numerous ferrocene-labeled H-1 were attracted to a magnet and the residual probes in the supernatant solution resulted in an obvious decease of peak current. Taking advantages of the homogeneous electrochemical detection and enzyme-free signal amplification, the constructed DNA biosensor showed wide linear range, low detection limit, and excellent selectivity in discriminating mismatched base sequences, which may provide a promising approach to develop sensitive nucleic acid sensing platforms in the fields of bioanalysis.

2. Experimental section

2.1. Materials and chemicals

Tetraethyl orthosilicate (TEOS), anhydrous sodium acetate, ethylene glycol, (3-aminopropyl)triethoxysilane (APTES), ammonium hydroxide ($NH_3 \cdot H_2O$, 28 wt%), and iron(III) chloride hexahydrate ($FeCl_3 \cdot 6H_2O$) were obtained from Sinopharm Chemical Reagent Co., Ltd. (China). N-hydroxysuccinimide (NHS) and

1-ethyl-3-(3-(dimethylamino)propyl) carbodiimide (EDC) were bought from Sigma-Aldrich Chemical Co. (USA). Carboxymethyl-β-cyclodextrin (CM-β-CD) was purchased from Zhiyuan Biotechnology Co., Ltd. (China). All other chemicals involved in the experiments were of analytical purity and commercially available, and utilized without any additional treatment. Phosphate buffered (PB, 10 mM) solution for dissolving all oligonucleotides was prepared by mixing appropriate proportions of Na_2HPO_4 and NaH_2PO_4, and the pH was regulated by the further addition of NaOH or H_3PO_4. DNA oligonucleotides designed in this paper were synthesized and purified by Dalian Takara Biomedical Technology Co., Ltd. (China) and the base sequences of all oligonucleotides were listed as follows. Dual ferrocene-labeled hairpin probe (H-1): 5′-Fc-GCG ATC GGA ACG TTC AGC TGC TAC CAT CGA CTC CCG TTC CGA TCG C-Fc-3′. Fluorescent hairpin probe (H-2): 5′-FAM-GCG ATC GGA ACG TTC AGC TGC TAC CAT CGA CTC CCG TTC CGA TCG C-DABCYL-3′. Assist probe 1 (A-1): 5′-GCT GAA CGT TCC G-3′. Assist probe 2 (A-2): 5′-AGT CGA TGG TAG CA-3′. Target DNA: 5′-CGA TGG TAG CAG CTG AAC GTT C-3′. Single-base mismatched DNA: 5′-CGA TGG TAG CAT CTG AAC GTT C-3′. Non-complementary sequence: 5′-ACC TAC ATC CTC CAC ATC CAC C-3′. The DNA hybridization process was carried out in 10 mM Tris-HCl buffer solution (pH 7.5) containing 50 mM NaCl. Human serum samples were kindly supplied from the affiliated hospital of Yangzhou university and stored in a refrigerator at −20 °C before use. Ultrapure water with a resistivity of 18.2 MΩ·cm was collected by a Milli-Q water purification system (Millipore, USA) and served for the preparation of aqueous solutions.

2.2. Synthesis of pure Fe_3O_4 nanoparticles

Pure Fe_3O_4 nanoparticles were prepared via a facile solvothermal process (Deng et al., 2008). Briefly, anhydrous sodium acetate (3.60 g) and $FeCl_3 \cdot 6H_2O$ (1.35 g) were first added to 50 mL ethylene glycol and the mixture was vigorously stirred for 10 min to yield a yellow homogeneous solution. The acquired solution mixture was sealed into a Teflon-lined stainless steel autoclave (100 mL in volume) and solvothermally treated at 200 °C for 8 h. Then, the resultant black precipitates were collected by magnetic separation, rinsed with ethanol and ultrapure water for several times, and finally dried at 60 °C in a vacuum oven for 24 h.

2.3. Preparation of Fe_3O_4@SiO_2@β-CD nanocomposites

The preparation of Fe_3O_4@SiO_2@β-CD nanocomposites was performed as follows. First, the as-synthesized Fe_3O_4 particles (0.25 g) were suspended in 50 mL HCl aqueous solution (0.1 M) under ultrasonication, and the black solids were repeatedly rinsed with ultrapure water followed by dispersing in the 200 mL of solution mixture ($V_{ethanol}$:V_{water} = 4:1). Subsequently, 3 mL $NH_3 \cdot H_2O$ and 3 mL TEOS were added into the solution mixture and vigorously stirred at room temperature for 5 h. After rinsing again with ultrapure water, the resultant Fe_3O_4@SiO_2 nanoparticles were dispersed in the mixture of 2.5 mL ethanol and 0.5 mL APTES under vigorous stirring for 5 h, and then rinsed with excessive water to obtain the amino-functionalized Fe_3O_4@SiO_2 nanoparticles (Fe_3O_4@SiO_2-NH_2). Finally, Fe_3O_4@SiO_2-NH_2 and excess CM-β-CD were added to the PBS solution (pH 5.3) containing 20 mM NHS and 10 mM EDC and continuously stirred for 12 h at room temperature. The acquired products were thoroughly rinsed with ultrapure water and dried at 50 °C overnight.

2.4. Fabrication of electrochemical biosensor

Prior to the measurement, a bare glassy carbon electrode (3 mm in diameter) was successively polished with the slurries of alumina powder (1.0, 0.3, and 0.05 μm) on the cloth and repeatedly washed with ultrapure water until the mirror-like surface was obtained. Then, the electrode was cleaned with anhydrous ethanol and ultrapure water in an ultrasonic bath to thoroughly remove the residual alumina slurries and allowed to dry under nitrogen atmosphere. H-1 probe (1 μM) was annealed at 90 °C for 5 min and gradually cooled down to the room temperature to produce a stem-loop structure. Subsequently, the mixture of 1 μM A-1, 1 μM A-2, and target DNA at variable concentrations were added to the solutions and incubated for 45 min. After the addition of Fe_3O_4@SiO_2@β-CD, the resultant mixture was reacted at room temperature for 60 min and rapidly separated with the assistance of a magnet. Finally, the pre-treated electrode was placed in the obtained supernatant solution for the differential pulse voltammetry (DPV) detection with a pulse amplitude of 50 mV and a potential interval ranging from 0.05 to 0.5 V (vs. SCE).

3. Results and discussion

3.1. Characterizations of Fe_3O_4@SiO_2@β-CD nanocomposites

Magnetic Fe_3O_4 nanoparticles showed the characteristic diffraction peaks at 30.2°, 35.6°, 43.4°, 53.5°, 57.1°, and 62.7° (Fig. 1A), which were assigned to the (220), (311), (400), (422), (511), and (440) planes, respectively, of the inverse spinel-structured Fe_3O_4 (Gan et al., 2011; Wang et al., 2010). After being coated with silica shell, a broad and weak diffraction peak at about 22.8° appeared for Fe_3O_4@SiO_2 particles, confirming the generation of an amorphous silica layer (Shao et al., 2012; Sun et al., 2014). When the surfaces of Fe_3O_4@SiO_2 particles were further functionalized, Fe_3O_4@SiO_2@β-CD nanocomposites exhibited a nearly

identical diffraction profile to that of Fe_3O_4, which demonstrated that the crystal structure of Fe_3O_4 was not ruined during the process of successive surface modification.

As depicted in Fig. 1B, the values of magnetization saturation (M_s) for Fe_3O_4, Fe_3O_4@SiO_2, and Fe_3O_4@SiO_2@β-CD were determined to be 71.6, 42.1 and 39.8 emu g^{-1}, respectively. The gradually decreased M_s could be attributed to the relatively low content of magnetic components (Fe_3O_4) in the Fe_3O_4@SiO_2 and Fe_3O_4@SiO_2@β-CD nanocomposites, which was resulted from the introduction of SiO_2 shell and the further surface functionalization of β-CD on the Fe_3O_4 core.

Although the magnetic properties of Fe_3O_4@SiO_2@β-CD nanocomposites were lower than Fe_3O_4, fast aggregation of Fe_3O_4@SiO_2@β-CD nanocomposites from their homogeneous dispersion could be achieved within 20 s under the application of a magnet (Fig. S2). When the external magnetic field was removed, Fe_3O_4@SiO_2@β-CD nanocomposites were quickly re-dispersed by a gentle shaking. Thus, the obtained nanocomposites possessed outstanding magnetic responsivity, which played an important role in the subsequent electrochemical detection.

XPS analyses were applied to further provide the useful information about the elemental compositions of samples. Four predominant peaks at 103.1, 154.1, 285.1, and 533.1 eV were clearly observed from the survey scan (Fig. 1C), corresponding to the Si 2p, Si 2s, C 1s, and O 1s levels of Fe_3O_4@SiO_2@β-CD nanocomposites, respectively. The high-resolution XPS scan of Fe_3O_4 nanoparticles displayed doublet peaks of Fe $2p_{3/2}$ and Fe $2p_{1/2}$ at 710.6 and 724.1 eV, respectively (Fig. 1D). However, the characteristic peak intensities of Fe 2p were obviously decreased for Fe_3O_4@SiO_2, indicating that Fe_3O_4 cores were completely coated with the silica shells. After the subsequent modification of β-CD, the Fe 2p peaks of Fe_3O_4@SiO_2@β-CD

nanocomposites were further weakened and nearly invisible.

The TEM image of Fe_3O_4 nanoparticles clearly showed a quasi-spherical shape with a relatively rough surface and the mean particle size was found to be 385 nm (Fig. 2A,B). After the encapsulation of silica layer, a representative core–shell architecture of Fe_3O_4@SiO_2 with a shell thickness of ~27 nm was obtained (Fig. 2C,D). Compared with Fe_3O_4@SiO_2, Fe_3O_4@SiO_2@β-CD had a much rougher surface, revealing that numerous β-CD molecules were successfully linked to the surface of Fe_3O_4@SiO_2 nanoparticles (Fig. 2E,F).

3.2. Feasibility of electrochemical DNA biosensor

The fluorescence spectra of the DNA probe under different conditions were applied to evaluate the viability of the target-induced TSDR process, in which the hairpin probe (H-2) was dually labeled with a fluorophore (FAM) at its 5′-terminus and a quencher (DABCYL) at its 3′-terminus, respectively (Fig. S3). As shown in Fig. 3A, before target DNA was added, a weak fluorescence signal of H-2 was observed because of the formation of a stem-loop structure (curve a), which brought the quencher in close proximity with the fluorophore. After target DNA was added, the stem-loop structure of H-2 was partially opened, and thus the fluorescence intensity was slightly increased with the increase of reaction time (curve b). Similarly, a tiny change could be detected in the mixture of H-2, A-1, and A-2 owing to the existence of weak background signal (curve c). However, upon the subsequent introduction of target, the conformational change of H-2 initiated the TSDR process, and allowed assist probes to further hybridize with H-2 for the release of target sequence from the DNA duplex. The released target was available to bind with another H-2 and trigger the signal amplification, leading to a high fluorescence signal by the separation of

FAM from the DABCYL quencher (curve d), which revealed that TSDR as an amplifier could significantly enhance the signal response of detection system. Moreover, the fluorescence intensity gradually increased upon increase of reaction time and nearly arrived at a plateau after 45 min. Thus, 45 min was chosen for the efficient TSDR process, and the corresponding fluorescence spectra were displayed in Fig. 3B. Compared with different mixtures containing H-2 probe, the great fluorescence enhancement was only obtained in the coexistence of H-2, A-1, A-2 and target DNA, which was consistent with the results of Fig. 3A, confirming the successful assembly of TSDR.

To further clarify the feasibility of the developed electrochemical biosensor, DPV measurements in different reaction systems were recorded in Fig. 3C. In the presence of H-1 only, its stem-loop structure prevented the host-guest recognition of β-CD due to the principle of dimension matching. After magnetic separation, numerous H-1 remaining in the supernatant solution generated a strong DPV oxidation peak (curve a). Upon subsequent addition of assist probes, a negligible signal change was observed, which could be ascribed to the fact that the absence of target sequence limited the TSDR process (curve b). When target DNA was introduced to the reaction system, the DPV oxidation peak was significantly decreased, indicating that a lot of unfolded H-1 probes generated by the target-induced TSDR process were removed from the supernatant solution by the capture of Fe_3O_4@SiO_2@β-CD nanocomposites (curve c). According to the aforementioned results, we could draw a conclusion that it is feasible to utilize this fabricated electrochemical biosensor for the monitoring of target DNA.

3.3. Optimization of experimental parameter

The molecular recognition capability of β-CD directly affected analytical performances of the constructed biosensor. Taking this into account, the reaction time of host-guest interaction was investigated. As displayed in Fig. S4, with the augment of reaction time, the response signal gradually decreased, because the more unfolded H-1 probes were captured by Fe_3O_4@SiO_2@β-CD nanocomposites and separated from the supernatant solution under an external magnetic field. When the reaction time was up to 60 min, the current variation began to flatten, which indicated that the recognition reaction nearly reached a maximum. Thus, the reaction time of 60 min was recommended as the optimized experimental parameter in the subsequent electrochemical measurements.

3.4. Detection of DNA

The sensing performance of this homogeneous electrochemical system was studied by the incubation with target DNA at different concentrations under the optimized experimental conditions (Fig. 4). A distinct DPV oxidation peak was obtained and its response current decreased gradually with the elevated concentration of target DNA, demonstrating that our fabricated biosensor was significantly dependent on the analyte concentration. As illustrated in Fig. 4B, the current intensity (*I*) displayed a desirable linear negative correlation to the logarithm of DNA concentration ranging from 1 pM to 5 nM with a regression equation of I (μA) = −0.259 − 0.032lg([DNA]/M) (R^2 = 0.9952). In accordance with the 3σ rule (σ represents the standard deviation of several parallel measurements in blank solution), the detection limit was determined as 0.3 pM. Sensing performances of different DNA biosensors with other signal amplification techniques were compared in Table S1. Obviously, our performances including linear range, detection limit, and reaction time were

comparable to that of these recently reported DNA analytical systems. The low detection limit in this work could be ascribed to the high recognition capability of β-CD, efficient TSDR-mediated target recycling amplification reaction, and homogeneous electrochemical detection mode.

3.5 Reproducibility and selectivity of biosensor

The same batch and batch-to-batch detections were applied to test the reproducibility of the developed sensing strategy. The relative standard deviations of inter-assays for five independent electrodes and intra-assays at the same electrode for five measurements toward 0.5 nM target DNA were estimated to be 6.5 % and 3.6 %, respectively, which demonstrated that the developed biosensor possessed satisfactory reproducibility and could be ideal candidates for DNA detection in practical analysis.

Moreover, the anti-interference ability also played a major role in evaluating the practical application of the constructed biosensor in real samples. As shown in Fig. 5, selectivity experiments were performed by investigating the current responses toward perfectly complementary target and other interfering sequences, including single-base mismatched and non-complementary target sequences. A significant signal drop was obtained in the presence of target DNA, but no obvious current changes between the interfering sequences and blank solution could be observed, indicating that only target DNA could effectively hybridize with H-1 probe and trigger the TSDR process. Thus, the proposed sensing platform possessed good selectivity for target DNA determination.

3.6 Practical application of biosensor in complex system

In order to investigate the practical application of the designed biosensing approach

in complex systems, recovery tests were implemented by selecting human serum as a model. Prior to detection, all samples were diluted 50 times to improve the DNA hybridization efficiency, which avoided the influence of the highly concentrated tissue in human serum. A good recovery in the range of 96.4%−102.5% was obtained for the serum samples spiked with target DNA at different levels by the standard addition method (Table S2). These results confirmed the practical application of the fabricated electrochemical biosensor for DNA monitoring in complex biological samples.

Conclusions

A novel enzyme-free and homogeneous electrochemical analytical method for sensitive target DNA detection was achieved by the artful combination of the TSDR-induced target recycling and flexible host-guest interaction. The dual-labeled oligonucleotide probe easily underwent a hairpin-opening process in the homogeneous solution driven by the target-triggered TSDR. Numerous ferrocene-labeled probes could be included in the cavity of β-CD through the host-guest interaction and then separated from the supernatant solution by means of an external magnet. Consequently, residual probes resulted in an obvious decease of peak current. Through the integration of the high specificity of TSDR-assisted target recycling, excellent recognition capability of β-CD, and homogeneous electrochemical detection mode, the proposed biosensor showed satisfactory sensitivity and high selectivity for target DNA analysis and was successfully applied to work in real samples. This facile, reliable, and sensitive enzyme-free biosensor could be extended for the monitoring of other targets just by the substitution of appropriate probe sequences.

Acknowledgments

This work was financially supported by the National Natural Science Foundation of China (No. 21703199, 21773203, and 21511140282), Jiangsu Planned Projects for Postdoctoral Research Funds (No. 1601138C), and a project funded by the Priority Academic Program Development of Jiangsu Higher Education Institutions. The authors in this study also acknowledge the fervent assistance from the testing center of Yangzhou university for the characterizations of Fe_3O_4@SiO_2@β-CD nanocomposites.

Appendix A. Supplementary data

Supplementary data associated with this article can be found in the online version at http://dx.doi.org/10.1016/j.bios.xxxxxxxx.

References

Bi, S., Jia, X.Q., Ye, J.Y., Dong, Y., 2015. Biosens. Bioelectron. 71, 427−433.

Cai, Z.M., Chen, Y.Y., Lin, C.S., Wu, Y.F., Yang, C.J., Wang, Y.R., Chen, X., 2014. Biosens. Bioelectron. 61, 370−373.

Chen, C.H., Li, N.X., Lan, J.W., Ji, X.H., He, Z.K., 2016. Anal. Chim. Acta 902, 154−159.

Chen, M., Wang, Y.Y., Su, H.L., Mao, L., Jiang, X.N., Zhang, T., Dai, X.Z., 2018. Sens. Actuators B 255, 2910−2918.

Chen, Y., Xiang, Y., Yuan, R., Chai, Y.Q., 2015. Nanoscale 7, 981−986.

Deng, Y.H., Qi, D.W., Deng, C.H., Zhang, X.M., Zhao, D.Y., 2008. J. Am. Chem. Soc. 130, 28−29.

Diao, W., Tang, M., Ding, S.J., Li, X.M., Cheng, W.B., Mo, F., Yan, X.Y., Ma, H.M.,

Yan, Y.R., 2018. Biosens. Bioelectron. 100, 228−234.

Duan, R.X., Wang, B.Y., Hong, F., Zhang, T.C., Jia, Y.M., Huang, J.Y., Hakeem, A., Liu, N.N., Lou, X.D., Xia, F., 2015. Nanoscale 7, 5719−5725.

Fu, L.B., Tang, D.P., Zhuang, J.Y., Lai, W.Q., Que, X.H., Chen, G.N., 2013. Biosens. Bioelectron. 47, 106−112.

Gan, Q., Lu, X.Y., Yuan, Y.A., Qian, J.C., Zhou, H.J., Lu, X., Shi, J.L., Liu, C.S., 2011. Biomaterials 32, 1932−1942.

He, H.F., Dai, J.Y., Duan, Z.J., Zheng, B.Z., Meng, Y., Guo, Y., Xiao, D., 2016. Sci. Rep. 6, 30878.

He, S.J., Liu, K.K., Su, S., Yan, J., Mao, X.H., Wang, D.F., He, Y., Li, L.J., Song, S.P., Fan, C.H., 2012. Anal. Chem. 84, 4622−4627.

He, S.J., Song, B., Li, D., Zhu, C.F., Qi, W.P., Wen, Y.Q., Wang, L.H., Song, S.P., Fang, H.P., Fan, C.H., 2010. Adv. Funct. Mater. 20, 453−459.

Hu, R., Liu, T., Zhang, X.B., Huan, S.Y., Wu, C.C., Fu, T., Tan, W.H., 2014. Anal. Chem. 86, 5009−5016.

Huang, J., Wu, Y.R., Chen, Y., Zhu, Z., Yang, X.H., Yang, C.Y., Wang, K.M., Tan, W.H., 2011. Angew. Chem. Int. Ed. 50, 401−404.

Hun, X., Xie, G.L., Luo, X.L., 2015. Chem. Commun. 51, 7100−7103.

Khodakov, D.A., Khodakova, A.S., Linacre, A., Ellis, A.V., 2013. J. Am. Chem. Soc. 135, 5612−5619.

Li, C.X., Wang, H.Y., Shen, J., Tang, B., 2015. Anal. Chem. 87, 4283−4291.

Li, H.B., Wang, S.Q., Wu, Z.S., Xu, J.G., Shen, G.L., Yu, R.Q., 2016. Biosens. Bioelectron. 77, 879−885.

Li, M.J., Zheng, Y.N., Liang, W.B., Yuan, R., Chai, Y.Q., 2017. ACS Appl. Mater. Interfaces 9, 42111−42120.

Li, Y., Lei, C.C., Zeng, Y., Ji, X.T., Zhang, S.S., 2012. Chem. Commun. 48, 10892−10894.

Liu, S.F., Lin, Y., Liu, T., Cheng, C.B., Wei, W.J., Wang, L., Li, F., 2014. Biosens. Bioelectron. 56, 12−18.

Nie, J., Zhang, D.W., Tie, C., Zhou, Y.L., Zhang, X.X., 2014. Biosens. Bioelectron. 56, 237−242.

Shao, M.F., Ning, F.Y., Zhao, J.W., Wei, M., Evans, D.G., Duan, X., 2012. J. Am. Chem. Soc. 134, 1071−1077.

Shi, X.M., Fan, G.C., Shen, Q.M., Zhu, J.J., 2016. ACS Appl. Mater. Interfaces 8, 35091−35098.

Sun, J., Yu, G.L., Liu, L.L., Li, Z.F., Kan, Q.B., Huo, Q.S., Guan, J.Q., 2014. Catal. Sci. Technol. 4, 1246−1252.

Tan, C.L., Yu, P., Hu, Y.L., Chen, J.Z., Huang, Y., Cai, Y.Q., Luo, Z.M., Li, B., Lu, Q.P., Wang, L.H., Liu, Z., Zhang, H., 2015. J. Am. Chem. Soc. 137, 10430−10436.

Wang, S.Q., Yang, F., Jin, D., Dai, Q., Tu, J.Y., Liu, Y.J., Ning, Y., Zhang, G.J., 2017. Anal. Chem. 89, 5349−5356.

Wang, X.Z., Dong, S.S., Gai, P.P., Duan, R., Li, F., 2016. Biosens. Bioelectron. 82, 49−54.

Wang, Y., Shen, Y.H., Xie, A.J., Li, S.K., Wang, X.F., Cai, Y., 2010. J. Phys. Chem. C 114, 4297−4301.

Xiong, E.H., Yan, X.X., Zhang, X.H., Liu, Y.Q., Zhou, J.W., Chen, J.H., 2017. Biosens. Bioelectron. 87, 732−736.

Xu, H., Wu, D., Li, C.Q., Lu, Z., Liao, X.Y., Huang, J., Wu, Z.S., 2017. Biosens. Bioelectron. 90, 314−320.

Xu, L.J., Lei, Z.C., Li, J.X., Zong, C., Yang, C.Y., Ren, B., 2015. J. Am. Chem. Soc.

137, 5149−5154.

Xuan, F., Luo, X.T., Hsing, I.M., 2012. Anal. Chem. 84, 5216−5220.

Yu, C.Y., Yin, B.C., Wang, S.L., Xu, Z.G., Ye, B.C., 2014. Anal. Chem. 86, 7214−7218.

Yu, X., Zhang, Z.L., Zheng, S.Y., 2015. Biosens. Bioelectron. 520−526.

Yuan, L., Tu, W.W., Bao, J.C., Dai, Z.H., 2015. Anal. Chem. 87, 686−692.

Zang, Y., Lei, J.P., Hao, Q., Ju, H.X., 2016. Biosens. Bioelectron. 77, 557−564.

Zhang, D.Y., Seelig, G., 2011. Nat. Chem. 3, 103−113.

Zhang, G.Y., Deng, S.Y., Cai, W.R., Cosnier, S., Zhang, X.J., Shan, D., 2015. Anal. Chem. 87, 9093−9100.

Zhang, H., Li, M.X., Fan, M.X., Gu, J.X., Wu, P., Cai, C.X., 2014. Chem. Commun. 50, 2932−2934.

Zhang, S.X., Han, G.J., Xing, Z., Zhang, S.C., Zhang, X.R., 2014. Anal. Chem. 86, 3541−3547.

Zhao, W.W., Yu, P.P., Shan, Y., Wang, J., Xu, J.J., Chen, H.Y., 2012. Anal. Chem. 84, 5892−5897.

Zhu, J., Ding, Y.S., Liu, X.T., Wang, L., Jiang, W., 2014. Biosens. Bioelectron. 59, 276−281.

Zhu, J.B., Zhang, L.B., Li, T., Dong, S.J., Wang, E.K., 2013. Adv. Mater. 25, 2440−2444.

Fig. 1. (A) Wide-angle XRD analyses and (B) magnetic hysteresis loops of (a) unmodified Fe_3O_4, (b) Fe_3O_4@SiO_2, and (c) Fe_3O_4@SiO_2@β-CD nanocomposites. (C) XPS survey scan of Fe_3O_4@SiO_2@β-CD nanocomposites. (D) The high-resolution XPS scan of (a) pure Fe_3O_4, (b) Fe_3O_4@SiO_2, and (c) Fe_3O_4@SiO_2@β-CD nanocomposites in the Fe 2p region.

Fig. 2. (A, C, E) TEM images and (B, D, F) the corresponding magnified TEM images of (top) Fe_3O_4, (middle) Fe_3O_4@SiO_2, and (bottom) Fe_3O_4@SiO_2@β-CD nanocomposites.

Fig. 3. (A) Time-dependent fluorescence responses and (B) fluorescence emission spectra after incubation of 45 min at λ_{ex} of 495 nm in the buffer solutions containing (a) 0.1 μM H-2, (b) 0.1 μM H-2 and 5 nM target, (c) 0.1 μM H-2, 0.1 μM A-1, and 0.1 μM A-2, and (d) mixture c + 5 nM target. (C) DPV curves of the fabricated biosensing system under different conditions: (a) 1 μM H-1, (b) 1 μM H-1, 1 μM A-1, and 1 μM A-2, and (c) mixture b + 1 nM target.

Fig. 4. (A) DPV curves of the fabricated biosensing system toward (a) 1, (b) 10, (c) 100, (d) 1.0×10^3, (e) 5.0×10^3, and (f) 1.0×10^4 pM DNA. (B) Calibration curve of the peak current response versus the logarithm of target DNA concentration. The error bars denote standard deviations for five tests.

Fig. 5. Selectivity investigation of the constructed electrochemical biosensing system toward (a) blank, 0.1 nM of (b) non-complementary DNA, (c) single-base mismatched DNA, and (d) perfectly complementary target DNA sequences. The error bars denote standard deviations for five tests.

Scheme 1. Schematic representation of homogeneous electroanalytical system for DNA determination based on TSDR-induced signal amplification and host-guest interaction.

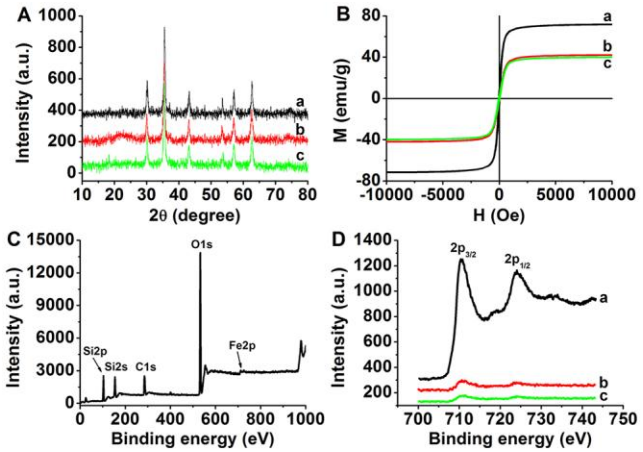

Fig. 1

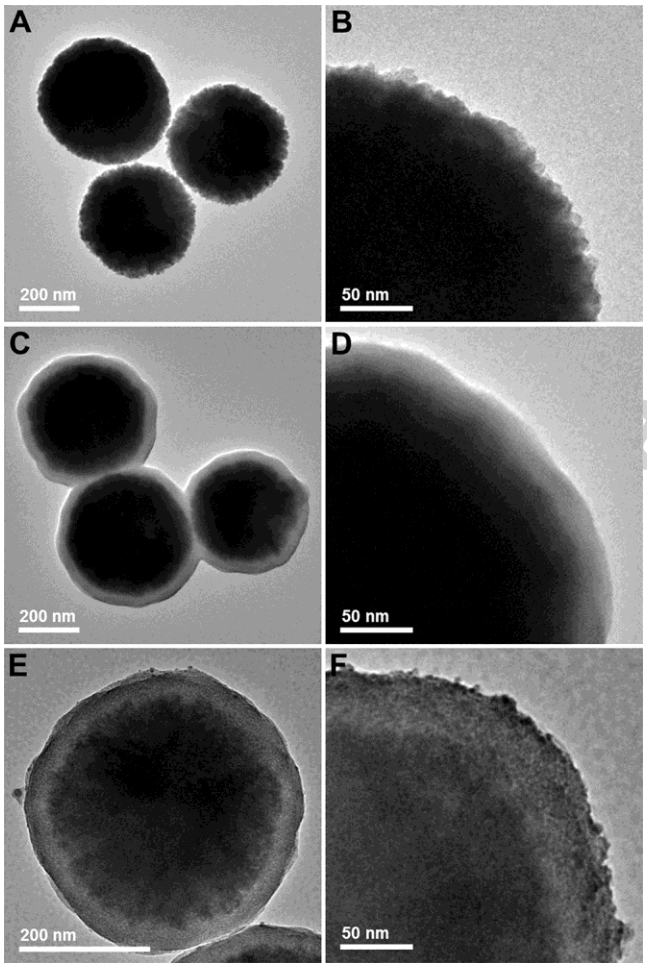

Fig. 2

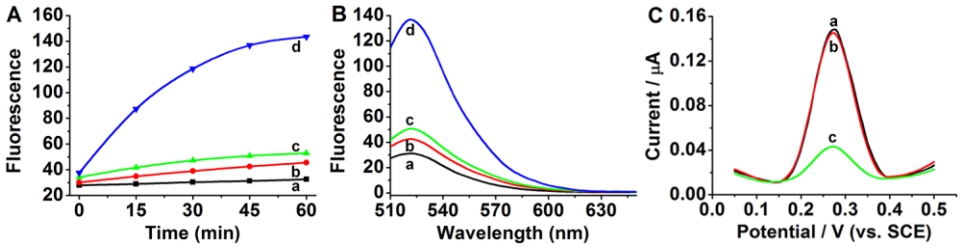

Fig. 3

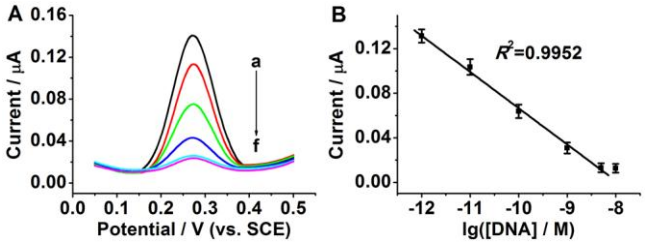

Fig. 4

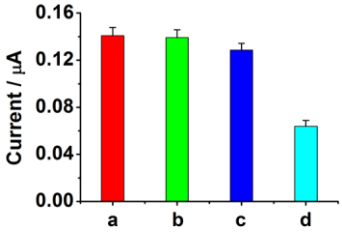

Fig. 5

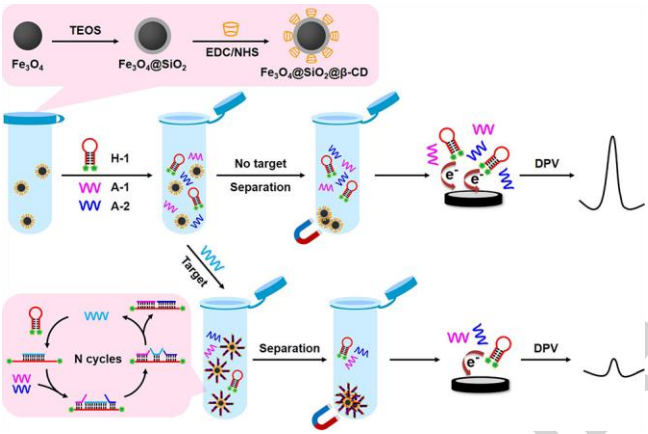

Scheme. 1

Highlights

- An enzyme-free homogeneous electrochemical sensing strategy was designed for sensitive DNA detection.
- The smart combination of TSDR-mediated signal amplification and host-guest recognition of Fe_3O_4@SiO_2@β-CD was utilized for the enhancement of detection sensitivity.
- The constructed biosensor showed wide linear range and excellent selectivity, and was successfully applied to the real sample analyses.